Opto-electronic and thermoelectric properties of double perovskites Na_2AgGaY_6 (Y = Cl, Br, I) for energy conversion applications: DFT calculations

S. Maqsood[a,*], S. Mumtaz[b], Y. M. Alanazi[c]
[a]*Centre for Advanced Studies in Physics (CASP), GC University, Lahore -54000.*
[b]*Department of Electrical and Biological Physics, Kwangwoon University, Seoul 01897, South Korea*
[c] *Department of Chemical Engineering, College of Engineering, King Saud University, Riyadh, 11451, King Saudi Arabia*

Double perovskites (DPs) that are both stable and environmentally sustainable are identified as an ideal choice for a broad range of applications, including thermoelectric and optoelectronic implementations. The current study investigates the complex physical characteristics of DPs Na_2AgGaY_6 (Y = Cl, Br, I) through the utilization of density functional theory (DFT), thus providing insights into its potential benefits in the fields of optoelectronics and thermal usage. The tolerance factor and Born's stability criteria are meticulously calculated in order to determine the structural stability of the cubic phase. The calculated direct band gap values for $Na_2AgGaCl_6$ and $Na_2AgGaBr_6$ ensure maximum absorption in the visible and infrared spectra, respectively. Na_2AgGaI_6 is the most optimal DP used in photovoltaic devices. An examination has been conducted on the See-beck coefficient, electrical and thermal conductivities, and other essential parameters utilized in the characterization of transport properties. The compounds Na_2AgGaI_6, $Na_2AgGaBr_6$ and $Na_2AgGaCl_6$ demonstrate exceptional ZT indices of 0.78, 0.74 and 0.73, accordingly, emphasizing their critical importance in thermoelectric devices.

(Received March 9, 2024; Accepted June 12, 2024)

Keywords: DFT investigations, Electronic properties, Mechanical properties, Absorption co-efficient, Figure of merit (ZT)

1. Introduction

Energy outages can serve as catalysts that generate attention towards energy resources. As energy consumption increases worldwide, the burden on current energy resources becomes more conspicuous. This escalates the likelihood of energy shortages, thus compelling researchers to investigate environmentally sustainable renewable energy sources. Solar energy provides a multitude of benefits, such as its scalability, sustainability, and minimal ecological footprint. These attributes are crucial in our pursuit of an autonomous source of power for communities and an environmentally friendly future [1, 2]. The efficacy of solar cells, which extract energy from radiation, is significantly influenced by the compounds employed [3]. In numerous ways, perovskites have been identified as advantageous compounds for this objective. Practical implementations of these compounds include their physical, optical, and electrical properties [4-6]. Double perovskites based on halides are appealing solid materials because of their prospective applications as insulators [7], photovoltaic energy absorbers [8-10], superconductors [11], and solar cell technology [12].

In the year 2019, endeavors to enhance the functionality of solar cells resulted in an increase in the conversion efficiency of solar energy to electricity beyond 24.2% by implementing lead-halide perovskites [13]. Following this, it is possible to increase the efficiency of solar cells by 47.1%. Kojima and his friends [14, 15] investigated the application of methyl-ammonium lead iodide ($CH_3NH_3PbI_3$) in solar cells. As a result of its disintegration into numerous compounds, $CH_3NH_3PbI_3$ was found to be extremely resistant to temperature fluctuations [16, 17]. Ion

* Corresponding author: saba.maq.55@gmail.com
https://doi.org/10.15251/DJNB.2024.192.919

exchange has been utilized by scientists to increase the operational lifetime of perovskite solar devices [18, 19]. As a result, Pb-free Double Perovskites halides emerge as the utmost viable options aimed at this objective. Opto-electronic usage, including LEDs as well as photovoltaic, has made use of Pb-based double perovskite halides intriguing, toxicology and insufficient stability preventing their widespread use in solar cells [20]. In order to address these concerns, scientists utilize cation blending and manufacturing techniques [21] to produce lead-free perovskites. The potential influence of the cation and anion combinations found in AMX_3 and its derivatives A_2MX_6 and A_2BMX_6 on magneto-electronic and photoelectric properties has been documented [22, 23]. A_2BMX_6 materials with band gap range exceeding 2eV have been the subject of research due to their potential as stable and non-toxic substances [24, 25]. To develop lead-free alternatives, further research has been conducted on perovskite compounds including silver and indium, given that gaping bands directly are intriguing. Subsequently, Volonakis and his group achieved success in their endeavors to produce $Cs_2AgInCl_6$, which possessed a band gap of 3.3 eV and remained vulnerable to ultraviolet radiation. It was proposed that Cs_2InAg $(Cl_{(6-x)}$ $Br_x)$ (where $x<1$) could be produced, taking into account experimental conditions and Goldschmidt's laws [25, 26]. Due to the everyday importance of conveyance devices, a considerable number of double perovskites have been investigated [27-31].

Chen et al. [32] investigated the stability and optoelectronic characteristics of double perovskites Li_2SbBiO_6 through the utilization of first-principle calculations. They discovered that Li_2SbBiO_6 satisfies the stability requirements and maintains $LiSbO_3$. Furthermore, they deliberated on their band gap as it pertains to visible radiation. An examination of the relationships between the pressure along with variations in related enthalpy as well as the thermoelectric formability (convex hull) regarding the non-magnetic material $Li_2BB'O_6$ (B′ = Se, Te, Mo, W; B = Ge, Hf, Ti, Hf, Zr, S,) was described in detail by Zhao et al. [33]. This study successfully isolated the double perovskite structures that could be synthesized. Furthermore, the identification of band gaps alongside ferroelectric reversing barriers for energy was accomplished through their Meta-stable crystal structures. Density functional calculations were employed to analyze the optical, electronic, thermoelectric, and stability properties of the halides Na_2AgGaY_6 (where Y represents Cl, Br, or I), drawing inspiration from double perovskites based on sodium. It has been confirmed that Na_2AgGaY_6 (Y = Cl, Br, I) is stable in its lowest energy state due to its high formation energy. The feasibility of utilizing double perovskites in optoelectronic devices is indicated by the existence of a significant absorption peak in the investigated samples. This peak, for instance, reveals electron transmission occurring directly between the valence band along with conduction bands. After conducting an extensive literature review on these materials, we are confident that the proposed research will provide a strong basis for experimenters and scholars to utilize Na_2AgGaY_6 (Y = Cl, Br, I) DPs in optoelectronic and thermoelectric applications.

2. Computational details

In order to study Na_2AgGaY_6 (Y=Cl, Br, I) halides, theoretical calculations are carried out to acquire structural information including photoelectric characteristics utilizing the full-potential linearized augmented plane wave (FP-LAPW+lo) method. The WIEN2k software was used for all simulations within the DFT paradigm [34]. In addition, the PBEsol-GGA [35] method was used to investigate mechanical variables and structural characteristics. Furthermore, the Trans-Blaha modified Becke-Johnson (TB-mBJ) potential was applied to ensure exact bandgaps [36] and accurate calculation of photoelectric properties [37], which aligns with the experiment's findings. Here, R_{MT} is the lowest muffin-tin radius while Kmax is the maximum value for the wave vector, thus, the alignment in the plane of wave ground to the internal energy barrier is identical. to $R_{MT}\times K_{max}$ = 8.0. The Brillion zone is where the investigation method is used for mechanical or electrical structures. In contrast, electrical and optical properties are investigated using the Monkhorst-Pack k-points [38] sample approach provides a 10×10×10 resolution for DOS. G_{max}= 16 $(a.u)^{-1}$ and l_{max}= 10, were the maximum values for the density of charges or wave functioning, respectively. In the middle of the Muffin-tin round, it had been anticipated that self-contained algorithms could achieve a point of convergent speed smaller than 0.0001|e| [39]. All parameters,

including the See-beck factor, the figure of merit, & temperature change with conductivity levels, were estimated using flexibility as well as the time frame for decreasing hypotheses [40] via the classical Boltzmann's equation.

3. Results and discussion

3.1. Structural and mechanical properties

Double perovskites have the chemical formulation $A_2BB'Y_6$, where BY_6 occupies an octahedral position and possesses the space group symmetry 225#Fm-3m [41]. The A-site atoms occupy the 8c location, whereas B-site atoms occupy the 4a position. Likewise, the halides inhabit the 24e Wyckoff position, whereas the B′-atom occupies the 4b position; the oxidation state for the halide ions Y is -1 [42]. As opposed to being univalent cations, A and B are trivalent (B′). As one of the double perovskites, Na_2AgGaY_6 (Y = Cl, Br, I) possesses a cubic structure and its unit cell contains the atoms Na (0.75, 0.25, 0.25), Ag (0, 0, 0), Ga (0.5, 0, 0), and Y (0.238, 0), which are positioned in perfect accordance with their respective positions. To determine the optimal state of the lattice capacity for the double perovskite under consideration, Na_2AgGaY_6 (Y = Cl, Br, I), the initial step involves calculating the combined energies of different volumes to feed each cell. In the case where the unit cell contains unconstrained atomic sites, the fundamental state to individual unit volume is obtained by ensuring that the threshold of atomic pull for every single atom is below 1 mRy/a.y. In place of defective stable perovskites, it is possible to obtain lead-free double perovskites. Figure 1 illustrates the double perovskites Na_2AgGaY_6, which take the form of cubes (Y = Cl, Br, I). The central atom of the octahedron-shaped structure is comprised of Ga or Ag. It is composed of Cl, Br, or I atoms.

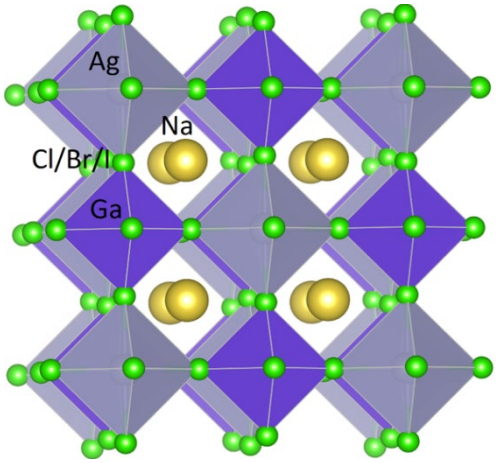

Fig. 1. Depicts the cubic unit cell of the halides Na_2AgGaY_6 (Y = Cl, Br, I) polyhedral format. The green color ball represents the Cl/Br/I atoms, the yellow color ball represents the Na atom, blue color and gray ball represent the Ga and In atoms, respectively.

To determine the physical rigidity of Na_2AgGaY_6 (Y = Cl, Br, I), the Goldschmidt factor (t_G) has been computed utilizing the elaborated atomic radii, as described in the following equation:

$$t_G = (r_{Na} + r_Y)/\sqrt{2\,(r_B + r_X)} \quad (1)$$

wherever r_{Li} is the radius of Na whereas r_Y includes radii of Y = Cl, Br, and I atoms, furthermore Y = Cl, Br, and I atoms ensure r_B as usual radii [43].To achieve maximum structure stability, t_G

need to be within the range of 0.8 to 1.04. In contrast, the t_G values of the investigated compounds are determined by the experimental data presented in Table 1.

Table 1. The lattice constant a_o(Å), bulk modulus B_o(GPa), tolerance factor (t_G), enthalpy of formation ΔH_f (eV), elastic constant (C_{11}(GPa), C_{12}(GPa), C_{44}(GPa)), shear m4odulus G(GPa), Young modulus Y (GPa), Pugh ratio B/G, anisotropy factor (A) and hardness (H_v) for cubic Na_2AgGaY_6 (Y = Cl, Br, I) calculated.

Parameters	$Na_2AgGaCl_6$	$Na_2AgGaBr_6$	Na_2AgGaI_6
	PBEsol	PBEsol	PBESol
a_o	9.94	10.55	11.43
B_o	40.08	32.95	24.22
t_G	0.98	0.97	0.95
ΔH_f	-2.84	-2.22	-1.93
C_{11}	80.94	64.86	28.49
C_{12}	18.77	15.55	24.85
C_{44}	16.75	13.74	18.78
B	39.49	31.98	26.06
G	21.91	17.40	7.98
Y	54.61	44.19	21.64
B/G	1.83	1.84	3.24
υ	0.269	0.270	0.36
A	0.54	0.56	0.60
H_v	4.18	3.47	1.04

The thermal durability is assessed by utilizing the amount of energy of formation (ΔH_f) as specified in the formula.

$$\Delta H_f = E_{\text{Total}}(Na_a Ag_b Ga_c Y_d) - aE_{Na} - bE_{Ag} - cE_{Ga} - dE_Y \quad (2)$$

(ΔH_f) is the transfer of energy from the lowest energy states of the investigated molecule to the energies of the components inside the unit cells. Whereas E_{Na}, E_{Ag}, E_{Ga}, and E_Y stand for the individual energies of the relevant compounds, E_{Total} represents the overall energy of the molecule. The atomic numbers of the elements are represented by the coefficients a, b, c, and d. Table 1 presents the entire results. With a negative energy of formation, our compounds are stable [44]. Based on their rising negative energies, Na_2AgGaI_6, $Na_2AgGaBr_6$ and $Na_2AgGaCl_6$ are inherently less stable than $Na_2AgGaCl_6$. This demonstrated the enhanced structure stability for the formulation constructed on I. Energy vs. volume plot was used to compute the ground state lattice constants (see Figure 2). Notably, when Cl was replaced with Br and I, the predicted a_o values increased significantly while the bulk modulus (B_o) decreased. This reduction is because the atomic radii of I and Br gradually grow as compared to Cl.

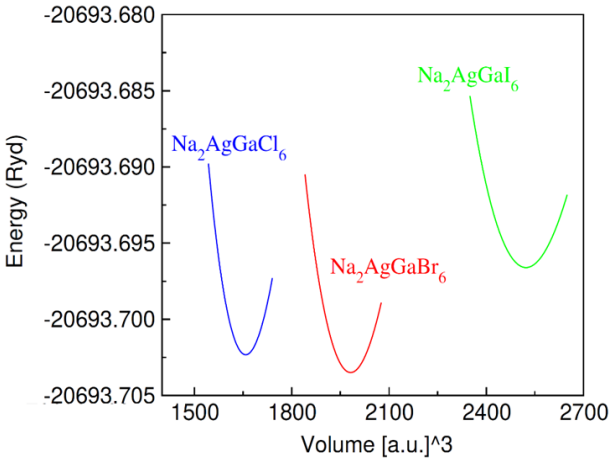

Fig. 2. Volume optimization of double perovskites under investigation Na_2AgGaY_6 (Y = Cl, Br, I).

A compound's anisotropy factor (A), modulus of elasticity (Y), Modulus of rigidity (G), including bulk modulus (B_o) determine its interatomic characteristics, such as its elasticity, stiffness, and durability [45]. Constants C_{11}, C_{12}, and C_{44} are the three separate elastic constants that can be used to quantify the aforementioned components. Table 1 displays the values for Na_2AgGaY_6 halides (where Y=Cl, Br, I), that encounter the elastically forte conditions: $C_{11} - C_{12} > 0$, $C_{11} + 2C_{12} > 0$ and $C_{12} < B < C_{11}$. Assortments of moduli, such as modulus of elasticity (Y), Modulus of rigidity (G), including bulk modulus (Bo), are employed to assess the tensile strength and stiffness of substances. In order to get a good picture of isotropic materials, the shear modulus along with bulk modulus has been intended using the Voigt-Reusse-Hill (VRH) method [46, 47]. To get the material's hardness (H_v), the following formula is used, following the procedure suggested by Tian et al. [48].

$$H_v = 0.92(G/B)^{1.137}(G)^{0.708} \quad (3)$$

Based on the data in Table 1, it can be concluded that $Na_2AgGaCl_6$ is a harder material compared to $Na_2AgGaBr_6$ and Na_2AgGaI_6, due to its higher Hv. The covalent nature of the bonds is shown by the substantially larger Young's modulus for $Na_2AgGaCl_6$. A material's ductility or brittleness may be determined by looking at Pugh's ratio B/G. The material is considered ductile if its B/G ratio is more than 1.75; otherwise, it is considered brittle. Ductility is demonstrated by the examined compound's B/G being larger than 1.75. Another measure of ductility is Poisson's ratio (υ), in the domain of elastic parameters, the isotropic properties are represented by the value 1 of the anisotropic factor (A), a crucial component. The anisotropic parameter's departure from 1 demonstrates that the longitudinal, shear, and elastic parameters are significantly different. This results in very anisotropic double perovskites denoted as Na_2AgGaY_6 (where X is either chlorine, bromine, or iron).

3.2. Opto-electronic properties

Energy band diagrams are essential in optoelectronic and thermoelectric systems, and they may be used to evaluate the performance of compounds. To determine the electrical band structure (BS) for the Na-centered halides Na_2AgGaY_6 (where Y is Cl, Br, or I), the TB-mBJ potential is used. Figure 3 depicts this BS. To modify the Fermi threshold at the Y position, an individual point computation using an increasingly dense k-mesh was necessary. Surprisingly, the band structure exists independently of the halogen component arrangement. The direct band gap is caused by the fact that $Na_2AgGaCl_6$ and $Na_2AgGaBr_6$ both have the same symmetric sites at. The metallic properties of Na_2AgGaI_6 are explained by its overlapping Fermi-level behavior. The improved performance of Na-based $Na_2AgGaCl_6$ and $Na_2AgGaBr_6$ has led to their extensive use in optoelectronic applications. Concerning the TB-mBJ potential, the direct energy gaps for

$Na_2AgGaCl_6$, and Na_2AgGaI_6 are 2.5 eV, 0.5 eV respectively and for $Na_2AgGaBr_6$ they are 1.6 eV. Among the compounds used in solar cells is $Na_2AgGaBr_6$. Ionic bonding generally has less of an impact on the narrowing of band gaps that occurs during a single Cl–I transition because of the larger atomic radii and lower electronegativity.

Moreover, the lowest and highest energy levels may be more easily simulated using the DOS graphs. In order to plot the Partial DOS along with Total DOS, all perovskite-based halides are being subjected to the mBJ potential. Pictured in Figure 3 is the partial density of the simulated states. It asserts that the V.B. consists of impurity p-states and 4-d Ag states, whilst the C.B is made up of 4-p Ga states.

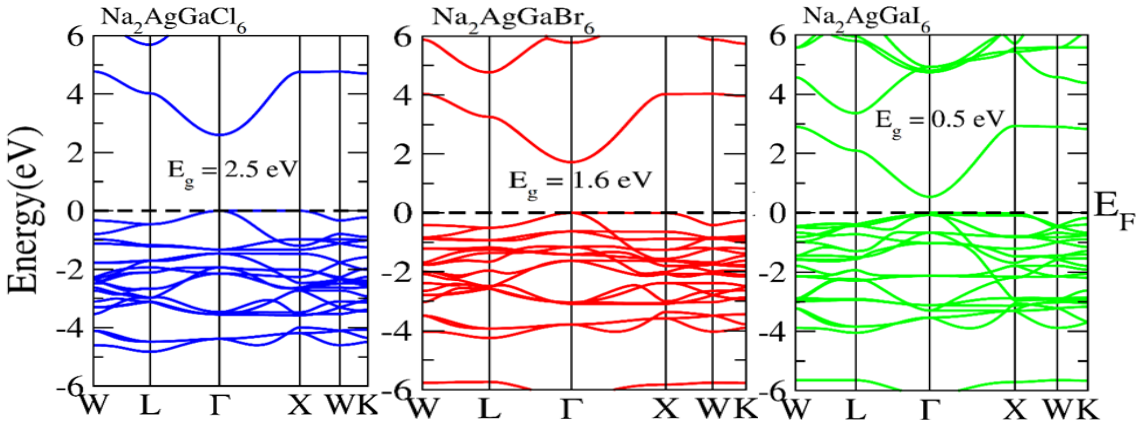

Fig. 3. Structure of the calculated electronic bands for the halides $Na_2AgGaCl_6$, $Na_2AgGaBr_6$ and Na_2AgGaI_6 with mBJ potential.

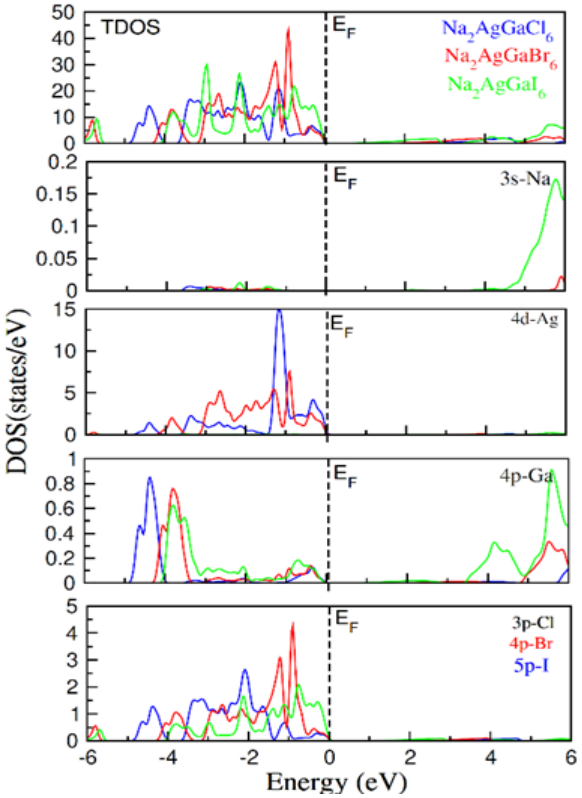

Fig. 4. Calculated total density of states (TDOS) of Na_2AgGaY_6 (Y = Cl, Br, I) and partial density of states of Na atom, Ga atom, In and Y atom with mBJ potential.

One of the most basic conditions for determining a substance's optical characteristics using Kramers-Kronig relations is that electromagnetic radiation induces electronic transitions in matter [49]. Input photons comprise a wavelength spectrum ranging from 0 to 12 eV. These dielectric constant's real $\varepsilon_1(\omega)$ and imaginary $\varepsilon_2(\omega)$ components have been found by using the Kramers-Kronig relation. Determined by graphing $\varepsilon_1(\omega)$ and $\varepsilon_2(\omega)$ versus energy within the prescribed period, a variety of optical characteristics for Na_2AgGaI_6, $Na_2AgGaCl_6$ and $Na_2AgGaBr_6$ were shown in Figure 5a-f. The metallic nature of DP Na_2AgGaI_6 prevents its optical properties from being studied in BS and DOS. The $\varepsilon_2(\omega)$ and $\varepsilon_1(\omega)$, symbols, respectively, represent the spectrum of light energy absorbed and radiation polarization, as mentioned in references [50, 51]. The graph shows that $\varepsilon_1(\omega)$ decreases for Na_2AgGaI_6, $Na_2AgGaBr_6$, and $Na_2AgGaCl_6$, before increasing and reaching its maximum values of 5.6 at 1.5eV, 3.2 at 3 eV, and 3.7 at 4.2 eV, correspondingly. It should be noted that when the energy lowers and atomic radii increase, the strength of the absorption peaks shows a rising trend from chlorine to bromine. In accordance with Penn's model equation $\varepsilon_1(0)\approx1+(\hbar\omega_p/E_g)^2$ [52], our static dielectric constant $\varepsilon_1(0)$, as displayed in Table 2, is suitable.

Table 2. The calculated indirect bandgap E_g (eV) with mBJ potential and optical parameters at 0 energy with mBJ for cubic Na_2AgGaY_6 (Y = Cl, Br, I).

	E_g(eV)	ε_1 (0)	*n* (0)	*R* (0)
$Na_2AgInCl_6$	2.5	2.8	1.6	0.06
$Na_2AgInBr_6$	1.6	3.2	1.8	0.08
Na_2AgInI_6	0.5	4.6	2.2	1.16

The $\varepsilon_2(\omega)$ is intricately connected to absorbance and plays a substantial role in determining the photonic characteristics of substances. The relationship between $\varepsilon_2(\omega)$ and energy values of up to 12 eV is illustrated in Figure 5(b). The computations of $\varepsilon_2(\omega)$ that emerge from the depiction are crucial as they are employed to determine the bandgaps among these combinations. Since $\varepsilon_2(\omega)$ is employed to ascertain the bandgaps of these materials, the results derived from the plot hold significant significance. Even though the estimated bandgap numbers and their corresponding band profiles vary to some degree. At 11 eV, the maximal value of $Na_2AgGaCl_6$ for $\varepsilon_2(\omega)$ is 6.0, while at 9.5 eV, it is 5.9 for $Na_2AgGaBr_6$ and at 7.8 eV it is 7.0 for Na_2AgGaI_6. Hence, owing to their efficacy as visible-range absorption, these metal halides are suggested for implementation in optoelectronic gadgets.

The scattering of light by the substrate is studied because the detection of light's velocity in a substance is reliant on its refractive index $n(\omega)$. At zero-point energy, the relationship between $n(\omega)$ and $\varepsilon_1(\omega)$ is demonstrated in Table 2 as $n^2(0) = \varepsilon_1(0)$. The values of $\varepsilon_1(\omega)$ and $n(\omega)$ are said to be energy-dependent. For $Na_2AgGaCl_6$, $Na_2AgGaBr_6$ and Na_2AgGaI_6 the first maximum values for $n(\omega)$ at 4.2 eV, 3.1 eV and 4eV, respectively, are 1.8, 2.2 and 2.5. Neither $Na_2AgGaCl_6$ nor $Na_2AgGaBr_6$ exhibits a parameter deviation smaller than 4 in the high-energy zone. When the substance's group velocity drops below its phase velocity, its metallic composition becomes apparent [53, 54]. If $n(\omega)$ stays between 1.0 and 3.0, as shown in Figure 5(c), it is deemed appropriate for optoelectronic equipment. $K(\omega)$ and $\varepsilon_2(\omega)$, the extinction parameters, behave similarly when it comes to the energy of entering photons. The highest points of $\varepsilon_2(\omega)$ represent an electrical movement from the valence and to the conduction band. The energy consumed for each unit length is represented by the absorption factor, which is abbreviated as $\alpha(\omega)$.

As illustrated in Figure 5(e), $\alpha(\omega)$ exhibits deflection in the presence of the light that enters Band gaps can be determined by analyzing multiple peaks within the absorbed spectrum spanning a high-energy range of 1 eV to 4 eV. The expected bandgap levels surpass the results derived from the arrangement of bands computation, which was restricted by the DFT exchanging potential and Kramers-Kronig formula calculations. The reliance on energy reflectivity $R(\omega)$

investigates its outermost layer contour. (Refer to Figure 5f). Because of its greater dimension and greater number of electrons, it grows from Chlorine to Br with a frequency of zero. Additionally, it exhibits an evident growth in the visible and infrared regions. Reflectivity thus indicates whether a substance is suitable for application in electronic equipment. The potential appeared through a standard visible-region contemplation that expanded.

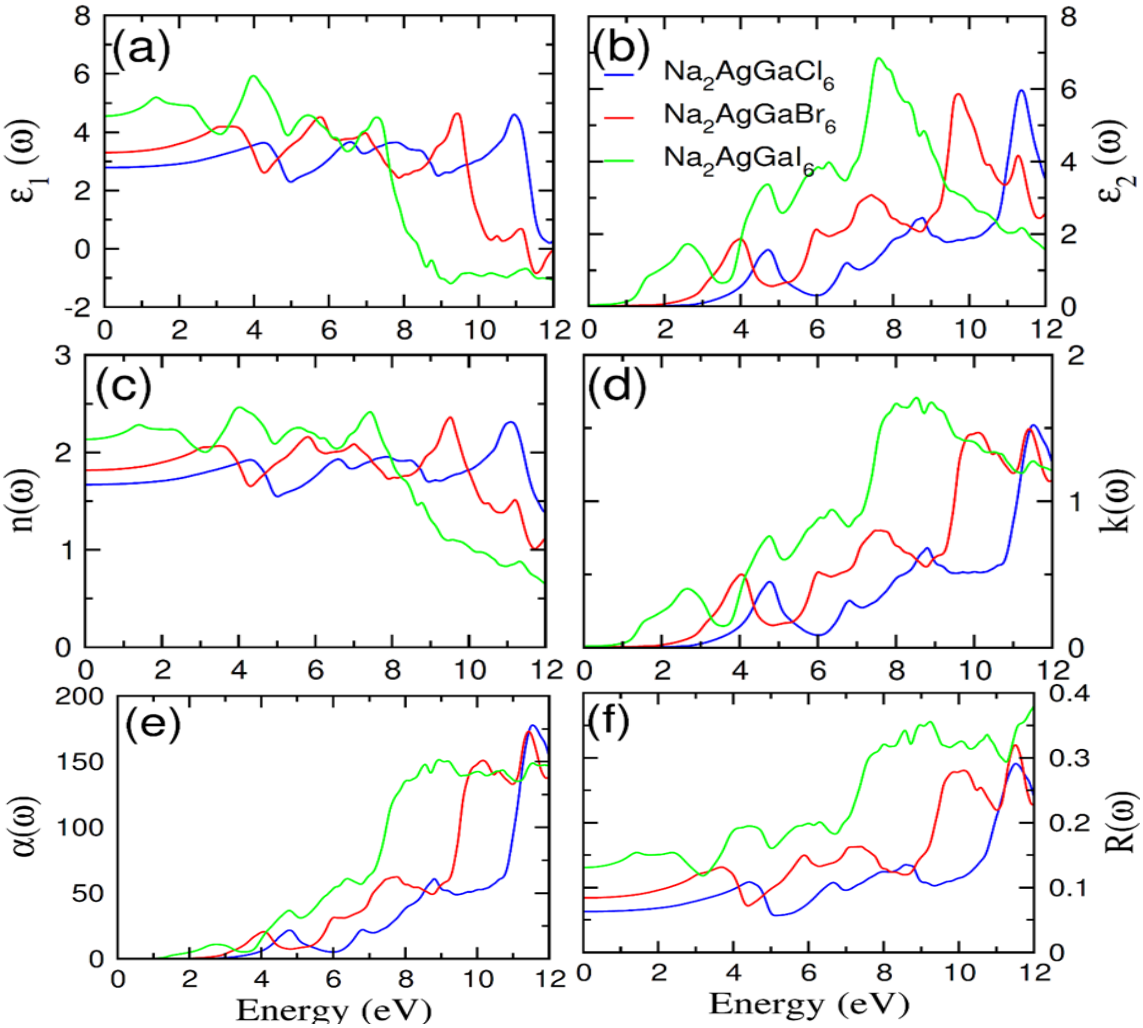

Fig. 5. The calculated (a) real part $\varepsilon_1(\omega)$, (b) imaginary part $\varepsilon_2(\omega)$ of the complex dielectric function, (c) refraction $n(\omega)$ and (d) extinction $k(\omega)$ co-efficient, (e) absorption $\alpha(\omega)$, (f) reflectivity $R(\omega)$ for Na_2AgGaY_6 (Y = Cl, Br, I).

3.3. Transport properties

As a result of gaining power, electrons in n-type and p-type semiconductors move from the V.B to the C.B, increasing the number of predominant carrying charges [55, 56]. To evaluate the thermal characteristics of sodium halides, the BoltzTraP algorithm is used. The link between warmth and electric conductivity is shown in Figure 6a, as band propagation and electromagnetic band gap are the determinants of transport characteristics. From 200K to 800K, the value of σ/τ for $Na_2AgGaCl_6/Na_2AgGaBr_6/Na_2AgGaI_6$, halides increases linearly, with ratios that range from $0{,}75/0.51/0.38\times10^{19}$ 1/(Ωms) to $2.08/1.12\times10^{19}$ 1/(Ωms). As the ambient temperature rises, there are additional carriers of charge in the range of conduction. The DP measurements for Cl-based halides are relatively bigger than those of Br-based halides up to 400K because Cl halides have larger atomic radii. One measure of a material's thermal performance is its Seebeck ratio. Figure 6(b) shows that bond breakdown at high temperatures causes the graph's rise exponentially from 300K to 600K. For $Na_2AgGaCl_6$, $Na_2AgGaBr_6$ and Na_2AgGaI_6 halides, the Seebeck coefficients

decreased from 180 μV/K, 190 μV/K and 230 μV/K at 300K to 185 μV/K, 168 μV/K and 215 μV/K at 600K, accordingly, indicating the orientation of the holes.

Based on the expression $\kappa = \kappa_e + \kappa_{ph}$ there are two methods for thermal conductivity to occur: one involves the transmission of heat via electrons, κ_e, and the other involves the phononic component of transferring heat, κ_{ph}. Due to constraints imposed by the BoltzTrap algorithm, we have just taken electron heat transfer into account. As shown in Figure 6c, the thermodynamic conduct coefficient (κ_e/τ) for Cl/Br/I, first rises nearly linearly from 1.25×10^{14} $Wm^{-1}Ks$ at 300 K to $4.1/4.0/5.8 \times 10^{14}$ $Wm^{-1}Ks$ at 600 K, respectively. Because Na_2AgGaI_6 has a lower bandgap than $Na_2AgGaCl_6$ and $Na_2AgGaBr_6$, its application results in a less pronounced rise in the coefficient of thermal conductivity. These materials have been determined to be suitable for thermoelectric purposes through computational analysis. Until 800K, Na_2AgGaI_6 exhibits greater values of (κ_e/τ) than $Na_2AgGaCl_6$ and $Na_2AgGaBr_6$ because the coulombs force and bond dissociation are unique.

For temperatures between 200K and 600K, we also calculate the heat capacity (C_v). Figure 6d shows that when the degree of heat increases, C_v for $Na_2AgGaCl_6$, $Na_2AgGaBr_6$ and Na_2AgGaI_6 likewise increases. The heat capacities C_v at ambient temperature for Cl and Br are 2.0 $Jmol^{-1}K^{-1}$ and 1.6 $Jmol^{-1}K^{-1}$, as well, as estimated. The Seebeck Factor measures the potential change that results from the heat gradient across the edges of various elements, also known as the Seebeck Phenomenon. The thermoelectric performance is represented by the power factor PF, which is PF = σS^2. This, plotted versus temperature, yields the figure of merit (ZT), as seen in Figure 6f. The ZT values for $Na_2AgGaCl_6$, $Na_2AgGaBr_6$, and Na_2AgGaI_6 halides grow across all temperature ranges of 200K to 600K because of a bigger Seebeck factor and a decrease in (κ_e/τ). The low levels of heat conduction give these substances their stability. Thus, the conductivity of heat has no influence on ZT. It is well-known that this top-notch thermoelectric compound has conflicting properties, such as a low κ_e/τ ratio and high electrical conductivity along with the Seebeck factor.

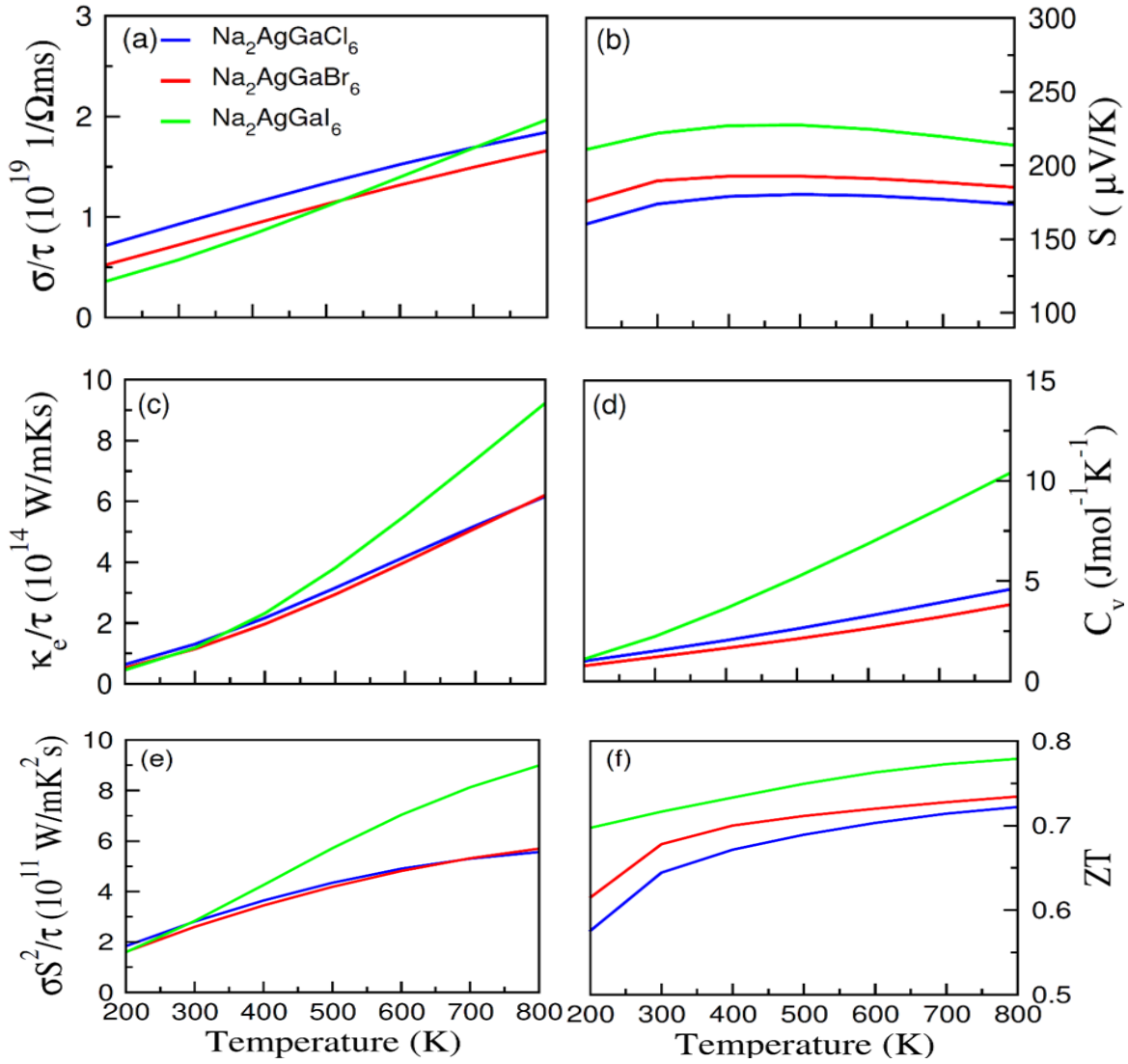

Fig. 6. The calculated (a) electrical conductivity (σ/τ), (b) thermal conductivity (k_e/τ), (c) Seebeck coefficients (S), (d) Specific heat capacity (Cv), (e) power factor and (f) figure of merit against temperature for Na_2AgGaY_6 (Y = Cl, Br, I)

4. Conclusion

In this study, we used PBEsol-GGA to study the structural integrity of this cubic form for Na-based perovskites Na_2AgGaY_6 (Y=Cl, Br, I) and compared our findings to known estimates of the ground state characteristics. Moreover, we computed the exact estimates of the optoelectronic characteristics of Na_2AgGaY_6 halides (X=Cl, Br, I) using the mBJ potential. The structural as well as thermodynamic stability of the aforementioned halides' regimes has been verified by determining their tolerance factor along with the energy of production.

According to the halide energy of production values (-2.84 eV for Cl, -2.22 eV for Br, and -1.93 eV for I), Na_2AgGaI_6 is more stable than $Na_2AgGaBr_6$ and $Na_2AgGaCl_6$, respectively. Halides are flexible because they have a high Poisson ratio (>0.26) and a high Pugh ratio (>1.75). The direct energy gap places halides in the optical to infrared spectrum, with Cl at 2.5 eV, Br at 1.6 eV, and I at 0.5 eV. For DPs $Na_2AgGaCl_6$, $Na_2AgGaBr_6$, Na_2AgGaI_6, respectively, and the dielectric value is used to evaluate the reflectivity or absorption. As the ambient temperature rises, the figure of merit for $Na_2AgGaCl_6$, $Na_2AgGaBr_6$, Na_2AgGaI_6 increases, indicating that these substances have great promise for thermoelectric applications.

Acknowledgements

The authors would like to acknowledge Researcher's Supporting Project Number (RSP2024R511), King Saud University, Riyadh, Saudi Arabia.

References

[1] Zhang, H., Zhu, X., Tai, Y., Zhou, J., Li, H., Li, Z., Lan, H., International Journal of Extreme Manufacturing, 2023, 5, 32005; https://doi.org/10.1088/2631-7990/acdc66

[2] Ye, S., Zhu, J., Zhu, S., Zhao, Y., Li, M., Huang, Z., He, J., ACS Applied Materials & Interfaces, 15 (2023), 47475-47486; https://doi.org/10.1021/acsami.3c09447

[3] Li, X., Liu, Y., Leng, J., Sustainable Materials and Technologies, 37 (2023) 00692; https://doi.org/10.1016/j.susmat.2023.e00692

[4] Yamada, T., et al., Advanced Materials, 2009. 21(13): p. 1363-1367; https://doi.org/10.1002/adma.200800253

[5] Lettieri, J., et al., Applied Physics Letters, 2000. 76(20): p. 2937-2939; https://doi.org/10.1063/1.126522

[6] Ghosh, S., S. Dasgupta, Materials Science-Poland, 2010. 28(2): p. 427-438.

[7] Zhu, Q., Chen, J., Gou, G., Chen, H., Li, P., Journal of Materials Processing Technology, 246 (2017) 267-275; https://doi.org/10.1016/j.jmatprotec.2017.03.022

[8] Huang, Z., Luo, P., Jia, S., Zheng, H., Lyu, Z, J. Physics and Chemistry of Solids, 167 (2022) 110746; https://doi.org/10.1016/j.jpcs.2022.110746

[9] Li, X., Aftab, S., Abbas, A., Hussain, S., Aslam, M., Kabir, F., Ansari, M. Z., Nano Energy, 2023, 118, 108979; https://doi.org/10.1016/j.nanoen.2023.108979

[10] Burschka, J., et al., Nature, 2013. 499(7458): p. 316-319; https://doi.org/10.1038/nature12340

[11] Takahashi, Y., et al., Dalton Transactions, 2011. 40(20): p. 5563-5568; https://doi.org/10.1039/c0dt01601b

[12] Aymen Nawaz, P., et al., Solar Energy, 2022. 231: 586-592; https://doi.org/10.1016/j.solener.2021.11.076

[13] Li, X., Aftab, S., Hussain, S., Kabir, F., Henaish, A. M. A., Al-Sehemi, A. G., Journal of Materials Chemistry A, (2024); https://doi.org/10.1039/D3TA06953B

[14] Wang, Y., Zhu, J., Li, M., Shao, G., Wang, H., Zhang, R., Materials & Design, 236 (2023) 112485; https://doi.org/10.1016/j.matdes.2023.112485

[15] Zhu, X., et al., Nature communications, 2019. 10(1): p. 1-10; https://doi.org/10.1038/s41467-019-10634-x

[16] Geisz, J.F., et al., IEEE Journal of Photovoltaics, 2018. 8(2): p. 626-632; https://doi.org/10.1109/JPHOTOV.2017.2778567

[17] Li, Z., et al., Advanced Functional Materials, 2019. 29(9): p. 1807280; https://doi.org/10.1002/adfm.201807280

[18] Zhang, Y.-Y., et al., Chinese Physics Letters, 2018. 35(3): p. 036104; https://doi.org/10.1088/0256-307X/35/3/036104

[19] Wu, M., et al., Journal of Materials Chemistry C, 2018. 6(43): p. 11575-11586; https://doi.org/10.1039/C8TC03926G

[20] Jiang, J., et al., The Journal of Physical Chemistry C, 2018. 122(31): p. 17660-17667; https://doi.org/10.1021/acs.jpcc.8b04013

[21] Zhang, Y., Liu, X., Song, M., & Qin, Z., Materials, 16 (2023) 2247; https://doi.org/10.3390/ma16062247

[22] Fu, Z. H., Yang, B. J., Shan, M. L., Li, T., Zhu, Z. Y., Ma, C. P., Gao, W., Corrosion Science, 164 (2020) 108337; https://doi.org/10.1016/j.corsci.2019.108337

[23] Muhammad, I., Ali, A., Zhou, L., Zhang, W., Wong, P. K. J., Journal of Alloys and Compounds, 909 (2022) 164797; https://doi.org/10.1016/j.jallcom.2022.164797
[24] Wang, H., Huang, Z., Zeng, X., Li, J., Zhang, Y., Hu, Q., ACS Applied Electronic Materials, 5 (2023), 3726-3732; https://doi.org/10.1021/acsaelm.3c00451
[25] Jacobsson, T.J., et al., The Journal of Physical Chemistry C, 2015. 119(46) 25673-25683; https://doi.org/10.1021/acs.jpcc.5b06436
[26] Volonakis, G., et al., The journal of physical chemistry letters, 2017. 8(4): p. 772-778; https://doi.org/10.1021/acs.jpclett.6b02682
[27] Manzoor, M., et al., Journal of Materials Research and Technology, 2022. 18: p. 4775-4785; https://doi.org/10.1016/j.jmrt.2022.04.073
[28] Mathew, N.P., N.R. Kumar, R. Radhakrishnan, Materials Today: Proceedings, 2020. 33: p. 1252-1256; https://doi.org/10.1016/j.matpr.2020.03.489
[29] Asghar, M., et al., Materials Science in Semiconductor Processing, 2022. 148: p. 106819; https://doi.org/10.1016/j.mssp.2022.106819
[30] Khan, M.A., et al., Solar Energy, 2021. 225: p. 122-128; https://doi.org/10.1016/j.solener.2021.07.026
[31] Aslam, F., B. Sabir, M. Hassan, Applied Physics A, 2021. 127(2): p. 1-12; https://doi.org/10.1007/s00339-020-04178-x
[32] Huang, Z., Luo, P., Wu, Q., & Zheng, H., J. Physics and Chemistry of Solids, 161 (2022) 110479; https://doi.org/10.1016/j.jpcs.2021.110479
[33] Zhao, M.H., Zhu, C., Sun, Z., Xia, T., Han, Y., Zeng, Y., Gao, Z., Gong, Y., Wang, X., Hong, J., Zhang, W.X., 2021, Chemistry of Materials, 34(1), pp.186-196.
[34] Blaha, P., et al., wien2k. An augmented plane wave+ local orbitals program for calculating crystal properties, 2001. 60.
[36] Tran, F., P. Blaha, Physical review letters, 2009. 102(22): p. 226401; https://doi.org/10.1103/PhysRevLett.102.226401
[37] Chen, J., Zhang, Z., Lu, H., Surfaces and Interfaces, 33 (2022) 102289; https://doi.org/10.1016/j.surfin.2022.102289
[38] Wisesa, P., K.A. McGill, T. Mueller, Physical Review B, 2016. 93(15): p. 155109; https://doi.org/10.1103/PhysRevB.93.155109
[39] Chen, X., Inorganics, 11(2023) 215; https://doi.org/10.3390/inorganics11050215
[40] Madsen, G.K., D.J. Singh, Computer Physics Communications, 2006. 175(1): p. 67-71; https://doi.org/10.1016/j.cpc.2006.03.007
[41] Usman, Muhammad, Qingfeng Yan, Crystals 10 (2020) 62. https://doi.org/10.3390/cryst10020062
[42] Bartel, C.J., et al., Science advances, 2019. 5(2): 0693; https://doi.org/10.1126/sciadv.aav0693
[43] Fedorovskiy, A.E., N.A. Drigo, M.K. Nazeeruddin, Small Methods, 2020. 4(5): p. 1900426; https://doi.org/10.1002/smtd.201900426
[44] Zhao, S., et al., Journal of Physics and Chemistry of Solids, 2018. 117: p. 117-121; https://doi.org/10.1016/j.jpcs.2018.02.032
[45] M. Jamal, S.J. Asadabadi, I. Ahmad, H.R. Aliabad, Comput. Mater. Sci. 95 (2014) 592-599; https://doi.org/10.1016/j.commatsci.2014.08.027
[46] Yang, B., Wang, H., Zhang, M., Jia, F., Liu, Y., Lu, Z., Chemical Engineering Journal, 476 (2023) 146834; https://doi.org/10.1016/j.cej.2023.146834
[47] Fu, S., Wu, H., He, W., Li, Q., Shan, C., Wang, J., Hu, C., Advanced Materials, 35 (2023), 2302954; https://doi.org/10.1002/adma.202302954
[48] R. Hill, Proc. Phys. Soc. 65 (1952) 349; https://doi.org/10.1088/0370-1298/65/5/307
[49] S. Pugh, Mag. J. Sci. 45 (1954) 823-843; https://doi.org/10.1080/14786440808520496
[50] Tian, Yongjun, Bo Xu, Zhisheng Zhao, International Journal of Refractory Metals and Hard Materials 33 (2012): 93-106; https://doi.org/10.1016/j.ijrmhm.2012.02.021

[51] Bobrov, V., et al., EPL (Europhysics Letters), 2010. 90(1): p. 10003; https://doi.org/10.1209/0295-5075/90/10003

[52] Noor, N., et al., Ceramics International, 2018. 44(12): p. 13750-13756; https://doi.org/10.1016/j.ceramint.2018.04.217

[53] Luo, Z., Cai, S., Hao, S., Bailey, T. P., Luo, Y., Luo, W. Kanatzidis, M. G., Extraordinary role of Zn in enhancing thermoelectric performance of Ga-doped n-type PbTe, 15 (2021); https://doi.org/10.1039/D1EE02986J

[54] Penn, D.R., Physical Review, 1962. 128(5): p. 2093; https://doi.org/10.1103/PhysRev.128.2093

[55] Zhang, Y., et al., RSC Advances, 2015. 5(25): p. 19647-19651; https://doi.org/10.1039/C4RA16506C

[56] Jiang, C., Deng, Z., Liu, B., Li, J., Han, Z., Ma, Y., Ma, Y., ACS Photonics, 9 (2022), 3089-3093; https://doi.org/10.1021/acsphotonics.2c00841